Journal of Power Sources 195 (2010) 1225–1234

Contents lists available at ScienceDirect

Journal of Power Sources

journal homepage: www.elsevier.com/locate/jpowsour

Using radial basis functions to approximate battery differential capacity and differential voltage

Jon P. Christophersen [a,*], Steven R. Shaw [b]

[a] Idaho National Laboratory, PO Box 1625, Idaho Falls, ID 83415, USA
[b] Montana State University, 610 Cobleigh Hall, Bozeman, MT, 59717, USA

ARTICLE INFO

Article history:
Received 28 July 2009
Received in revised form 27 August 2009
Accepted 28 August 2009
Available online 4 September 2009

Keywords:
Differential capacity
Differential voltage
Radial basis function
Bootstrapping
Lithium-ion

ABSTRACT

As part of the Department of Energy's Advanced Technology Development Program, lithium-ion cells of various sizes and chemistries are aged with periodic reference performance tests to ascertain degradation rates. The reference tests include a very slow discharge and charge based on a constant current equal to 1/25th of the rated capacity to elucidate the true electrochemical capacity of the cell. A differential analysis of these data helps to identify the individual kinetic and thermodynamic contributions of the anode and cathode. However, differential curves are very noisy, and previous smoothing methods included simple data reduction and moving averages. This paper introduces an alternative method of finding the differential voltage and differential capacity curves based on radial basis functions. The voltage profile is fit with a number of Gaussian curves, and the resulting model is differentiated. This approach also has the added advantage of assessing model uncertainty based on a bootstrap analysis. The radial basis function method was successfully applied to various lithium-ion chemistries tested under the Advanced Technology Development Program. The resulting differential capacity and differential voltage curves are generally smoother than the corresponding curves found by previous methods and also show little variance, indicating a good model fit. These results imply that the radial basis function technique is a more robust tool for assessing differential data.

Nomenclature

ATD	advanced technology development
β	Gaussian width
BOL	beginning of life
C_k	center locations/sampling interval
dQ/dV	differential capacity
dV/dQ	differential voltage
N	number of centers
NCA	nickel–cobalt–aluminum
NMC	nickel–manganese–cobalt
Q_{BOL}	beginning-of-life capacity
RBF	radial basis function
SOC	state-of-charge

1. Introduction

The use of advanced battery technologies is increasing as the United States seeks to reduce its dependence on foreign oil and find alternative energy resources. The automotive industry, for example, has been investigating lithium-ion chemistries for hybrid-electric and plug-in hybrid-electric vehicle applications. Consequently, the U.S. Department of Energy initiated the Advanced Technology Development (ATD) Program to address the barriers that are limiting the successful commercialization of lithium-ion batteries for vehicular use [1]. These barriers include accurate prognostic methods, abuse tolerance, cost, and low temperature performance [2].

As part of the ATD Program, prototype lithium-ion cells of various chemistries and configurations are aged using both standardized and exploratory methods, followed by a destructive diagnostic assessment to elucidate degradation mechanisms [1,2]. Cell chemistries for the second and third generation of ATD cells (i.e., Gen2 and Gen3 cells) are shown in Tables 1 and 2, respectively. The Gen2 cell chemistry consisted of a baseline nickel–cobalt–aluminum (NCA) mixture, and a variant chemistry (Variant C) with a positive electrode that contained an increased aluminum dopant and corresponding drop in cobalt. The cells were cylindrical, 18650-size (i.e., 18 mm diameter and 65 mm length)

* Corresponding author. Tel.: +1 208 526 4280; fax: +1 208 526 0690.
E-mail address: jon.christophersen@inl.gov (J.P. Christophersen).

0378-7753/$ – see front matter © 2009 Elsevier B.V. All rights reserved.
doi:10.1016/j.jpowsour.2009.08.094

Table 1
Gen2 cell chemistry and ratings.

	Gen 2 cells (18650)	
	Baseline	Variant C
Positive electrode	8 wt% PVDF binder 4 wt% SFG-6 graphite 4 wt% carbon black 84 wt% $LiNi_{0.8}Co_{0.15}Al_{0.05}O_2$	8 wt% PVDF binder 4 wt% SFG-6 graphite 4 wt% carbon black 84 wt% $LiNi_{0.8}Co_{0.1}Al_{0.1}O_2$
Negative electrode	8 wt% PVDF binder 92 wt% MAG-10 graphite	8 wt% PVDF binder 92 wt% MAG-10 graphite
Electrolyte	1.2 M $LiPF_6$ in EC:EMC (3:7 wt%)	1.2 M $LiPF_6$ in EC:EMC (3:7 wt%)
Separator	25 μm thick PE (Celgard)	25 μm thick PE (Celgard)
Rated capacity	1 Ah	0.8 Ah
Electrode area	846.3 cm^2	846.3 cm^2
Maximum voltage	4.1 V	4.1 V
Minimum voltage	3.0 V	3.0 V

with a voltage rage of 4.1–3.0 V. The beginning of life (BOL) rated capacities for the Baseline and Variant C cells were 1.0 and 0.8 Ah, respectively (at the 1-h rate). The Gen3 cells consisted of a baseline nickel–manganese–cobalt (NMC) mixture, and a variant chemistry (Variant A) that included 2% $LiBF_2C_2O_4$ as an electrolyte additive. These cells consisted of a prismatic design (35 mm width by 62 mm length) with a 400 mAh rated capacity and an 18650-configuration with a rated capacity of 800 mAh. The Gen3 voltage range was between 4.0 and 3.0 V.

Both the Gen2 and Gen3 cells were aged using standardized cycle-life or calendar-life profiles. Cycle-life testing consisted of continuous pulsing centered on a fixed state-of-charge (SOC) and test temperature. Calendar-life testing consisted of a voltage clamp at a fixed SOC and temperature [1–4]. Life testing was interrupted every four weeks for reference performance tests to gauge battery degradation in capacity, impedance, energy, and power at a given temperature (e.g. 25 °C). As part of the reference performance test, most cells were subjected to a $C_1/25$ test, consisting of a full discharge and charge using a constant current corresponding to 1/25th of the rated capacity. For example, a Gen2 Baseline cell with a rated capacity of 1 Ah required a $C_1/25$ discharge and charge constant current of 40 mA. Data were typically recorded every 30 s during this test to successfully capture the voltage behavior as a function of state-of-charge. The purpose of this test was to get a sense of the true electrochemical capacity of the cell as it degraded due to calendar- or cycle-life aging under pseudo-equilibrium conditions [2]. Additionally, the $C_1/25$ data were used to assess differential capacity or differential voltage. The advantage of differential analysis is the ability to isolate thermodynamic and kinetic information from the individual electrodes within a full cell where no reference electrode is present. Bloom et al. [5–8] used differential analysis to elucidate the primary source of capacity loss during aging for the Gen2 and Gen3 cells. Electrode materials from both fresh and aged cells were harvested and placed in half cells with a lithium–metal counter electrode to determine the degradation of both the cathode and anode [9,10]. These data were then used to isolate peak contributions of the individual electrodes within a full cell, and the subsequent peak shifts during aging were useful in identifying the source of capacity fade. It was determined that most of the capacity loss for the Gen2 and Gen3 cells was due to side reactions at the anode [5–8].

2. Experimental

2.1. Differential analysis

Fig. 1a shows the $C_1/25$ discharge curves measured at 25 °C for representative Gen2 and Gen3 cells at BOL. The representative Gen2 Baseline and Variant C cells showed very similar electrochemical capacities (1.07 and 1.03 Ah, respectively) though their rated capacities at the 1-h rate were 20% different. The Gen3 Variant A prismatic cell showed 0.47 Ah of available capacity, and the corresponding 18650-size cell yielded 0.79 Ah. Fig. 1b shows the $C_1/25$ charge curves for the same representative cells at BOL. The charge capacities differ slightly from the discharge values due to the voltage recovery during the 1-h rest at open-circuit prior to the charge (i.e., note that the starting charge voltage for each cell is higher than 3.0 V). Each of these curves monotonically increases in accumulated capacity as the voltage changes and show a sharp "knee" near full discharge.

Table 2
Gen3 cell chemistry and ratings.

	Gen 3 cells (Variant A)	
	Prismatic	18650
Positive electrode	8 wt% PVDF binder 8 wt% Super P carbon black 84 wt% $Li_{1.05}(Ni_{1/3}Co_{1/3}Mn_{1/3})_{0.95}O_2$	8 wt% PVDF binder 8 wt% Super P carbon black 84 wt% $Li_{1.05}(Ni_{1/3}Co_{1/3}Mn_{1/3})_{0.95}O_2$
Negative electrode	8 wt% PVDF binder 92 wt% (MCMB) 10–28	8 wt% PVDF binder 92 wt% (MCMB) 10–28
Electrolyte	1.2 M $LiPF_6$ in EC:EMC (3:7 wt%) 2% $LiBF_2C_2O_4$ additive	1.2 M $LiPF_6$ in EC:EMC (3:7 wt%) 2% $LiBF_2C_2O_4$ additive
Separator	25 μm thick PE	25 μm thick PE
Rated capacity	0.4 Ah	0.8 Ah
Electrode area	377 cm^2	486 cm^2
Max voltage	4.0 V	4.0 V
Min voltage	3.0 V	3.0 V

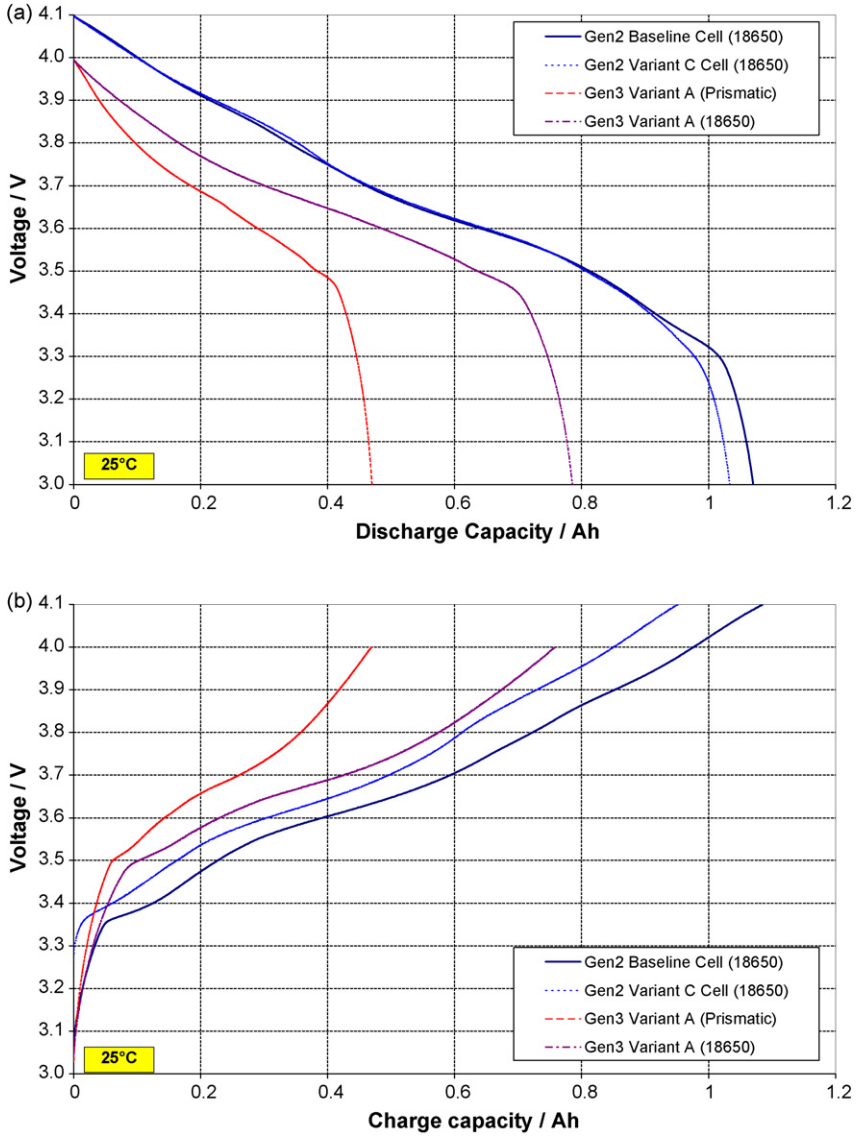

Fig. 1. (a) $C_1/25$ discharge curves for representative Gen2 and Gen3 cells. (b) $C_1/25$ charge curves for representative Gen2 and Gen3 cells.

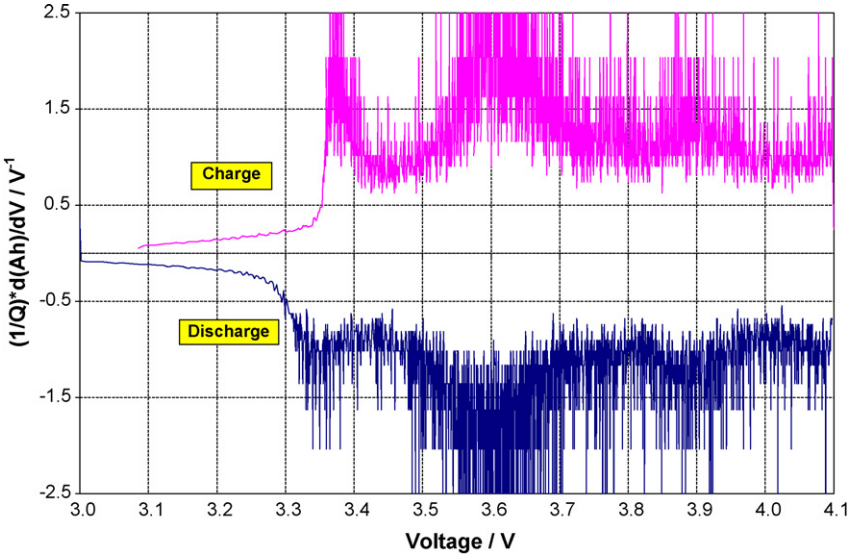

Fig. 2. Differential capacity discharge and charge curves at BOL for a representative Gen2 Baseline cell.

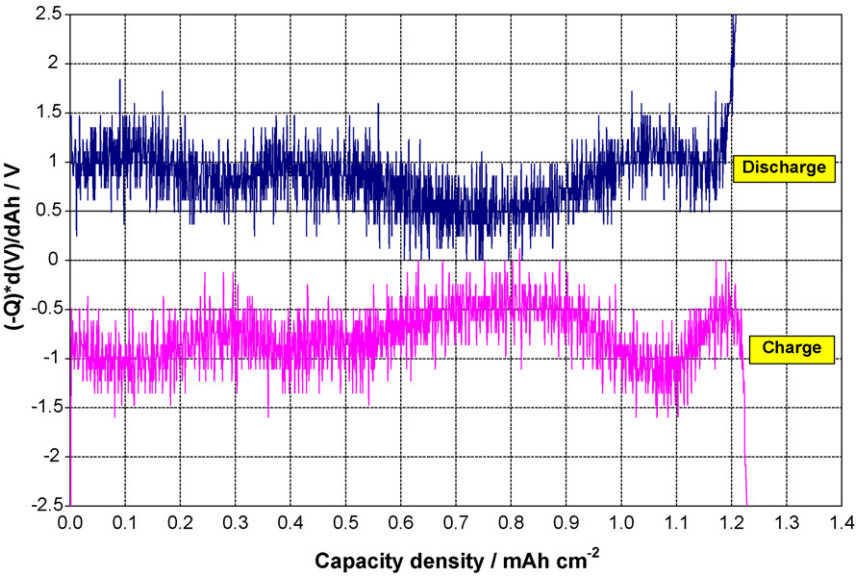

Fig. 3. Differential voltage discharge and charge curves at BOL for a representative Gen2 Baseline cell.

Differential capacity is defined in Eq. (1) as the relative change in capacity (ΔQ) over the corresponding voltage range (ΔV), scaled by the average BOL $C_1/25$ capacity (i.e., Q_{BOL}). Differential voltage is defined in Eq. (2) as the inverse of differential capacity. The peaks of the differential capacity curves (dQ/dV) represent phase equilibria, and the peaks from differential voltage (dV/dQ) represent phase transitions [5]. Figs. 2 and 3 show the resulting dQ/dV and dV/dQ curves, respectively, based on a simple two-point numerical differentiation for both the charge and discharge profiles of a representative Gen2 Baseline cell at BOL. Since measurements were typically collected at 30-s intervals, this approach yielded very noisy data. Additionally, differential capacity analysis can become problematic within some voltage regions when ΔV becomes very small for a corresponding change in capacity (ΔQ), resulting in a near-infinite solution. Consequently, Bloom et al. [5–8] focused on an analysis of differential voltage curves since ΔQ is never zero due to the constant current input. Another advantage of differential voltage is that the individual contributions of the cathode and anode can be combined linearly since the total cell voltage is simply the difference between the cathode and anode voltages [5].

$$\frac{dQ}{dV} = \frac{1}{Q_{BOL}}\frac{\Delta Q}{\Delta V} = \frac{1}{Q_{BOL}}\left(\frac{Q_t - Q_{t-1}}{V_t - V_{t-1}}\right) \tag{1}$$

$$\frac{dV}{dQ} = Q_{BOL}\frac{\Delta V}{\Delta Q} = Q_{BOL}\left(\frac{V_t - V_{t-1}}{Q_t - Q_{t-1}}\right) \tag{2}$$

Obviously, the $C_1/25$ data must first be smoothed prior to isolating peak locations and correlating them with electrode behavior. Various methods have been introduced, including a simple five-point moving average [5], or data reduction prior to taking the derivative (i.e., using the capacity measured every ninth minute and the average voltage in that 9-min interval, followed by a three-point numerical differentiation) [2]. Figs. 4 and 5 show the smoothed differential capacity and voltage curves, respectively, for the same representative Gen2 Baseline cell at BOL based on the data reduction method. The curves are significantly smoother and the peak locations are more clearly defined. However, these smoothing techniques are not very robust, and could be improved with a statistically based modeling approach. This paper presents an alternative method of calculating differential capacity and differential voltage using radial basis functions.

2.2. Radial basis function analysis

In the absence of a physical model for the $C_1/25$ discharge and charge curve (i.e., Fig. 1), an approach that combines parametric, black-box models with model order selection and bootstrapping was implemented using a Gaussian radial basis function (RBF) [11]. The objective was to estimate dQ/dV and dV/dQ curves from current and voltage measurements as a function of time. Using differential voltage as an example, the dV/dQ ratio can be split as shown in Eq. (3). Since the capacity, Q, is in units of amp-hours (Ah), the ratio of dQ/dt is simply the average constant current, $\bar{I}$, applied during the $C_1/25$ test. Consequently, the radial basis function only needs to be fit to the voltage data.

$$\frac{dV}{dQ} = \frac{dV/dt}{dQ/dt} = \frac{dV/dt}{d(It)/dt} = \frac{dV/dt}{\bar{I}} \tag{3}$$

To approximate dV/dt, the measured voltage as a function of time [i.e., $v(t)$], can be first expressed by Eq. (4), where v_0 and w are detrending parameters, and the summation function is composed of kernels, ϕ, that are evenly spaced by a sampling interval C_k, that is derived from the total number of centers, N. The argument of ϕ is called a radial basis function since it depends only on the radius from the independent variable, t, to the center of each function, C_k [11]. This model is applied to the observed voltage data to determine the fitting parameters of v_0, w, and a_k using least-squares estimation techniques. The resulting parameter estimates are then used in the derivative expression to approximate dV/dt.

$$v(t) = v_0 + wt + \sum_{k=1}^{N} a_k \phi(t - C_k) \tag{4}$$

The kernel ϕ can be expressed as the Gaussian function shown in Eq. (5), where β controls the width of the curve. The derivative of $\phi(x)$ is shown in Eq. (6).

$$\phi(x) = e^{-x^2/\beta} \tag{5}$$

$$\frac{d}{dx}\phi(x) = \frac{-2x}{\beta}e^{-x^2/\beta} = \frac{-2x}{\beta}\phi(x) \tag{6}$$

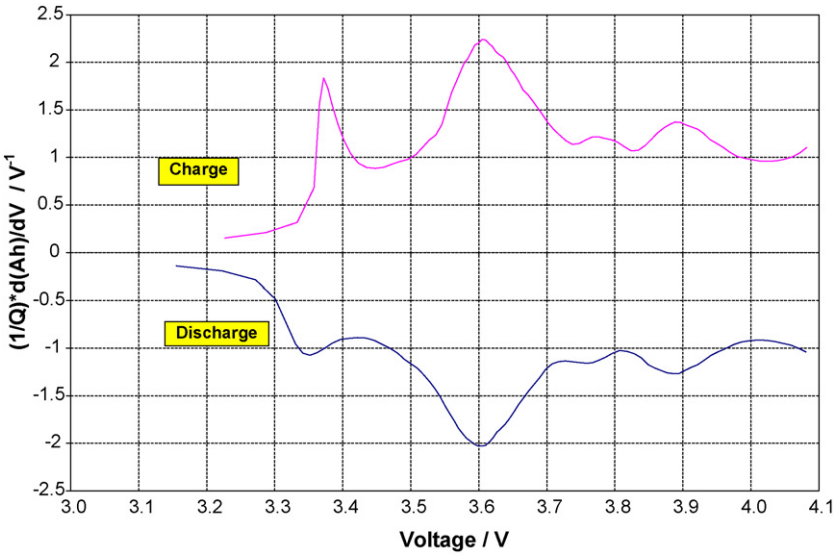

Fig. 4. Smoothed differential capacity discharge and charge curves at BOL for a representative Gen2 Baseline cell.

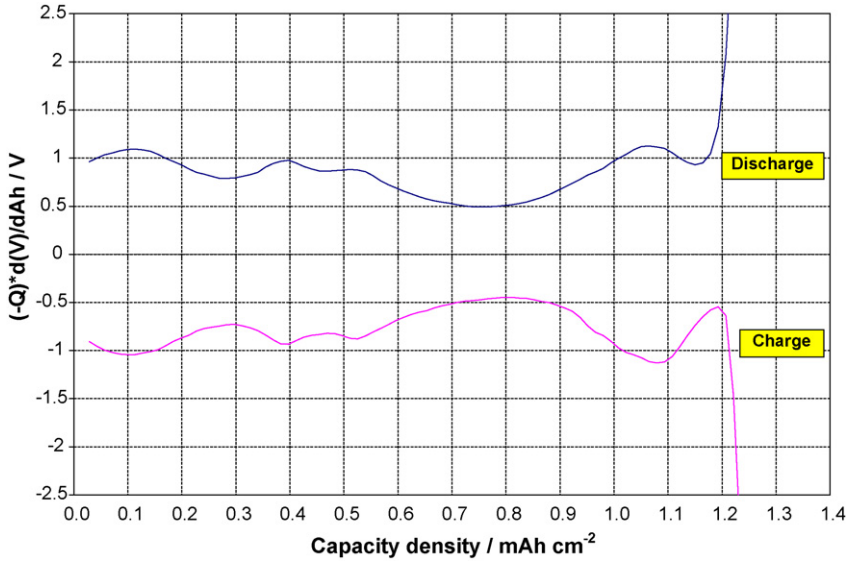

Fig. 5. Smoothed differential voltage discharge and charge curves at BOL for a representative Gen2 Baseline cell.

Therefore, the derivative of $v(t)$ in Eq. (4) can be written as shown in Eq. (7).

$$\frac{d}{dt}v(t) = w + \frac{d}{dt}\sum_{k=1}^{N} a_k \phi(t - C_k) = w + \sum_{k=1}^{N} a_k \frac{d}{dt}\phi(t - C_k) \tag{7}$$

Substituting the derivative of $\phi(x)$ yields Eq. (8). This derivative has an interesting form since it may also be written as shown in Eq. (9), where the first summation in the expression is simply the radial basis function portion of $v(t)$. An interesting observation is that the Gaussian kernel, $\phi(x)$, achieves local support and is also an eigenfunction of the derivative.

$$\frac{d}{dt}v(t) = w + \sum_{k=1}^{N} a_k \frac{-2(t - C_k)}{\beta}\phi(t - C_k) \tag{8}$$

$$\frac{d}{dt}v(t) = w + \frac{-2t}{\beta}\sum_{k=1}^{N} a_k \phi(t - C_k) + \frac{2}{\beta}\sum_{k=1}^{N} C_k a_k \phi(t - C_k) \tag{9}$$

Therefore, an estimate of the differential voltage curve can be described by combining Eqs. (3) and (9), as shown in Eq. (10).

$$\frac{dV}{dQ} = \frac{(d/dt)v(t)}{(dq(t)/dt)} = \frac{w + (-2t/\beta)\sum_{k=1}^{N} a_k \phi(t - C_k) + (2/\beta)\sum_{k=1}^{N} C_k a_k \phi(t - C_k)}{I} \tag{10}$$

The model structure, i.e., the values for the Gaussian width (β), number of centers (N), and center locations (C_k), can be used to adjust the tradeoff between capturing detail and reducing noise sensitivity when approximating $v(t)$ in Eq. (4). In system identification, this tradeoff is known as model order selection, and several criteria are available [e.g., 12,13]. These criteria typically involve comparing the number of parameters (i.e., centers in this case) with the approximation error. The approximation error goes to zero as the number of free parameters approaches the number of data points. Fig. 6 shows a residual norm ($|e|_2$) curve for the representative Gen2 and Gen3 cells at BOL over a range of 10–60 centers. Generally, a low number of centers results in underfitting (i.e., loss of curve detail), and a high number of centers causes overfitting (i.e., too much noise included in the fit) [11]. From Fig. 6, it is evident that the Gen2 Baseline cells have less noise than the other chemistries,

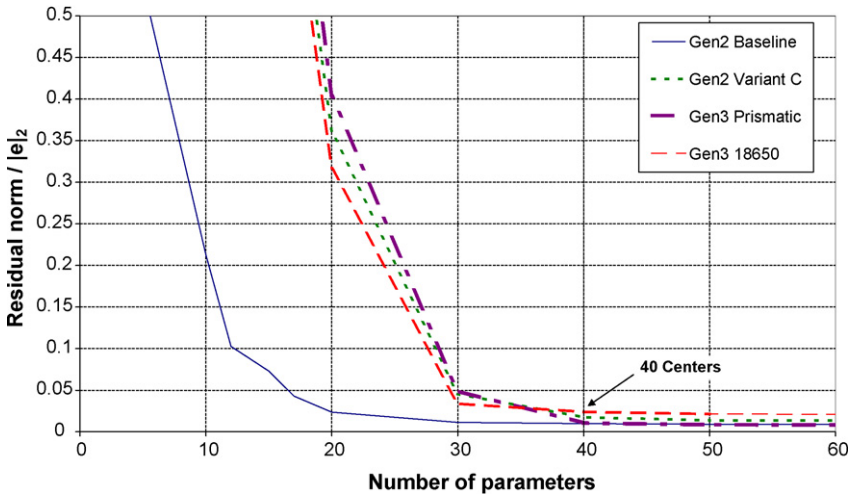

Fig. 6. Residual norm for radial basis function at various parameter values.

and the remaining representative cells seem to stabilize around $N = 40$ centers (however, the error will eventually drop to zero as N continues to increase since the noise would also be included in the fit). Consequently, $N = 40$ centers appears to be a good choice for both the Gen2 and Gen3 differential analysis. The center locations (C_k) are evenly spaced in N increments over a range that extends slightly beyond the total length of the voltage dataset (i.e., the voltage data points at the extremes are not unequally weighted by the Gaussian radial basis fit). Finally, the value of the Gaussian width (β) must be chosen such that the analysis does not yield a matrix calculation resulting in singular values. Otherwise, the resulting model fit is not overly sensitive to β, but it should be chosen such that it accounts for differences in sampling rates. A width value of 10,000 was chosen for the Gen2 and Gen3 cells in this analysis.

Parameter estimation using radial basis functions is a linear least-squares problem with a global, unique solution. Thus, the entire voltage dataset can be used to determine the differential curve, as opposed to the previous methods of simply throwing data away and/or smoothing based on moving averages. Additionally, the RBF model is tolerant of missing data points, so the bootstrap technique [14] can be used to estimate the *uncertainty* in dQ/dV and dV/dQ for a given model structure. The bootstrap is essentially a numerical equivalent of repeated experiments. The original data set is randomly re-sampled, with replacement, into a synthetic data set. Each original data point may occur once, twice, multiple times, or not all in the re-sampled dataset. This re-sampling procedure incorporates the underlying stochastic properties of the noise, which are not well known. Model parameters are then computed for the re-sampled data set to create an ensemble of "bootstrapped" dQ/dV and dV/dQ estimates, which can be summarized by calculating the sample variance. This uncertainty assessment is a distinct advantage of the RBF method since the error variance can not be assessed using the original data reduction or smoothing techniques.

3. Results and discussion

3.1. Voltage model fit

The error between the original voltage data and the model fit for the representative Gen2 and Gen3 cells at BOL is summarized in Table 3. All four fits show an error with zero mean and a standard deviation less than ±0.5 mV. The maximum difference observed was less than +4 mV for the discharge curve and −10 mV for the charge curve. Given a voltage range between ~4 V and 3 V, the resulting maximum error was less than 0.25%. Therefore, these data demonstrate that the RBF fit is able to successfully capture the voltage behavior.

Table 3
Error between voltage dataset and model fit (in mV).

Error	Gen2 cells		Gen3 cells	
	Baseline	Variant C	Prismatic	18650
Discharge (mV)				
Average	3.67E−10	−1.13E−12	1.63E−13	6.76E−13
St. Dev.	0.247	0.280	0.177	0.414
Maximum	3.519	1.101	1.969	1.864
Minimum	−1.711	−1.346	−0.723	−1.419
Charge (mV)				
Average	1.97E−09	2.64E−12	−1.14E−12	−1.25E−12
St. Dev.	0.328	0.317	0.280	0.403
Maximum	2.020	2.830	1.616	1.759
Minimum	−4.493	−9.986	−1.563	−2.794

3.2. Differential Analysis—Gen2 cells

Fig. 7a shows the differential capacity curve for the representative Gen2 Baseline cell at BOL based on the RBF model compared to the original data reduction method (see Fig. 4). Fig. 7b shows the corresponding differential voltage curves. Both methods appear to yield similar results, with peaks at roughly the same voltage locations, but there are also some subtle differences. From the dQ/dV curve (Fig. 7a), the RBF method yields a much sharper initial charge peak near 3.4 V with an amplitude of ~2.5 V^{-1}, followed by another "bump" with an amplitude of ~1.5 V^{-1}. The same behavior can be observed in the dV/dQ charge curve (Fig. 7b) near 1.2 mAh/cm^2. These features had been washed out with the original data reduction approach. Additionally, the RBF method appears to better preserve detail at the extremes. The high voltage peaks for both the discharge and charge curve (e.g., near 4.1 V on the dQ/dV curve or near 0.01 mAh cm^{-2} on the dV/dQ curve) seem better defined. However, the associated variances of these additional peaks are also relatively large (see below), which should be taken into consideration when isolating the contributions of individual electrodes. Similar results were also observed for the representative Gen2 Variant C cell (not shown in this paper).

The added advantage of the RBF fit is the ability to assess model variance. Fig. 8a and b show the bootstrap variance of the dQ/dV and dV/dQ curves, respectively, for the same Gen2 Baseline cell at BOL. The variance at the extremes is higher due to the inherent nature of the randomized sampling method. The parameter

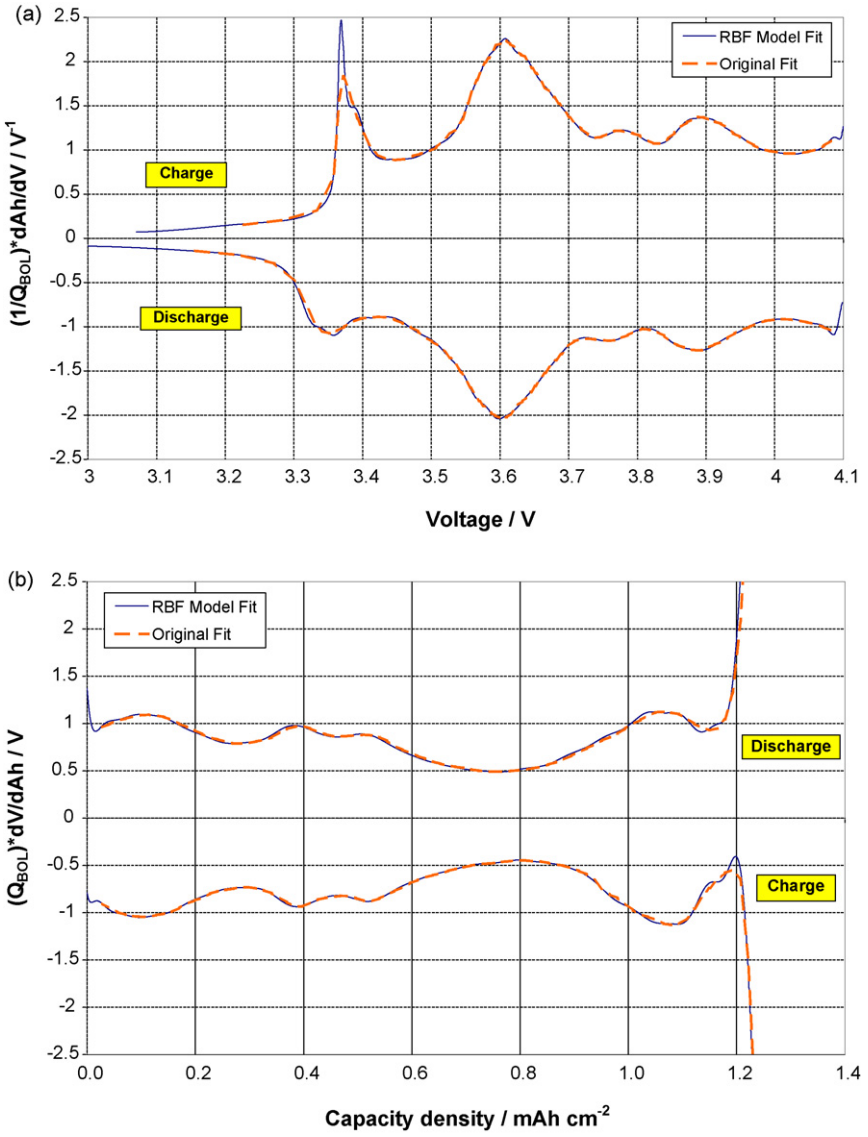

Fig. 7. (a) Comparison of dQ/dV analysis methods (RBF vs. data reduction) for a Gen2 Baseline cell at BOL. (b) Comparison of dV/dQ analysis methods (RBF vs. data reduction) for a Gen2 Baseline cell at BOL.

Table 4
Average bootstrap variance of the representative Gen2 cells.

	Baseline cell		Variant C cell	
	dQ/dV	dV/dQ	dQ/dV	dV/dQ
Discharge	4.12 mV^{-1}	1.69 μV	3.61 mV^{-1}	0.23 μV
Charge	6.63 mV^{-1}	2.15 μV	5.06 mV^{-1}	0.61 μV

estimates will essentially stay the same if the excluded data have adjacent points that are similar and included in the sample set (i.e., in the mid-voltage region). However, the voltage behavior shows a sharp "knee" near full discharge and an "uptick" near full charge (see Fig. 1). When data points at these locations are excluded in the randomized sample, the subsequent parameter estimates will show much more variability.

A summary of the average bootstrap variances for both the representative Gen2 Baseline and Variant C cells at BOL are summarized in Table 4. The differential capacity curves have an average variance less than ±7 mV^{-1}, and the differential voltage curves have average variances less than ±2.5 μV, indicating a very good model fit. Interestingly, the dQ/dV variance (Fig. 8a) also shows a sharp peak for the charge curve near 3.4 V, corresponding to the location of the initial charge peak in Fig. 7a. This indicates that higher noise content is present, making it more difficult to resolve the peak. However, the maximum variance at this voltage is only ~3.5% (approximately 85 mV^{-1} variance for a peak height of 2.5 V^{-1}), indicating that the RBF fit is still very good at this point. Likewise, the noise content of the dV/dQ curve also starts increasing near 1.2 mAh cm^{-2}.

3.3. Differential analysis—Gen3 cells

The dQ/dV curve for the representative 18650-size Gen3 Variant A cell at BOL is shown Fig. 9. Using the original data reduction technique, the differential curves are significantly noisier than the corresponding Gen2 cells, making it more difficult to identify peak locations. The only way to get a smoother curve would be to eliminate even more data at the expense of preserving subtle curve characteristics. Using the RBF approach with the same Gaussian width (β = 10,000) and number of centers (N = 40), however, the fit

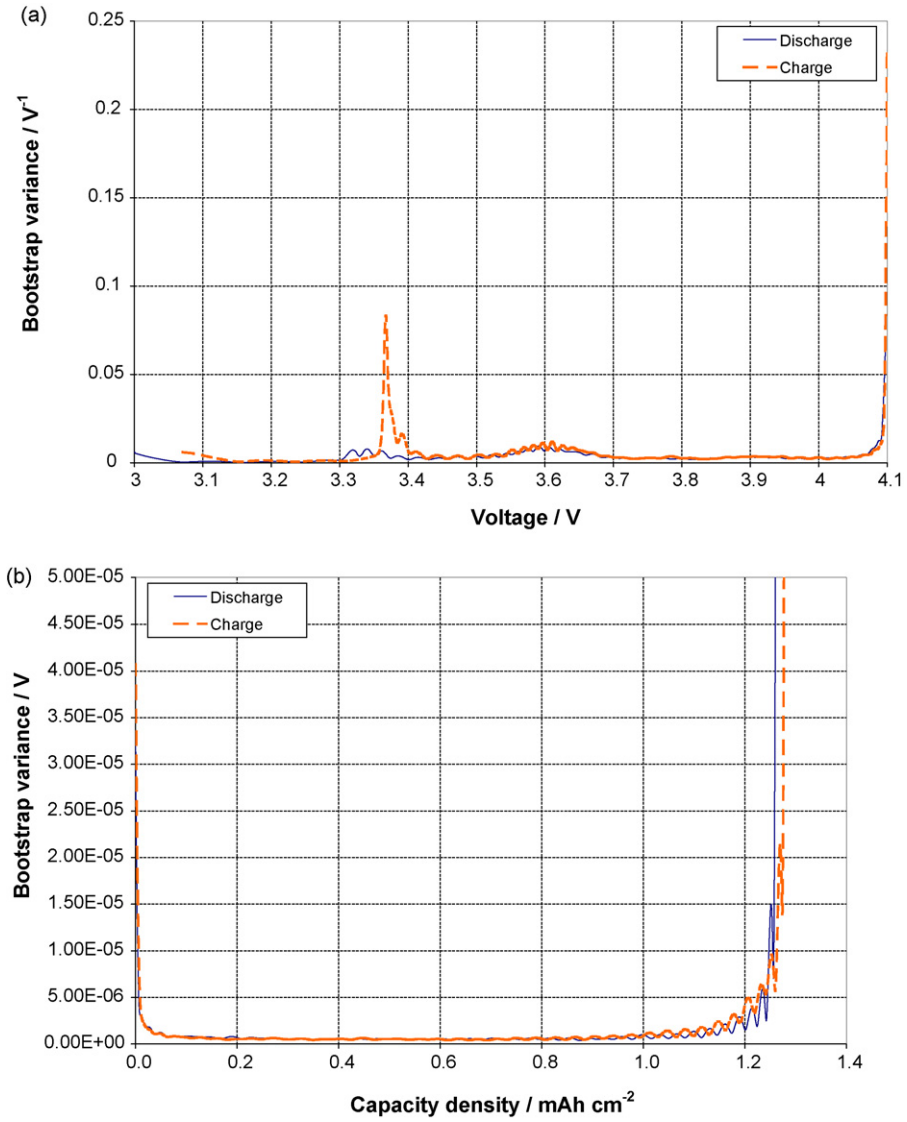

Fig. 8. (a) Bootstrap variance analysis for the *dQ*/*dV* curve of a Gen2 Baseline cell at BOL. (b) Bootstrap variance analysis for the *dV*/*dQ* curve of a Gen2 Baseline cell at BOL.

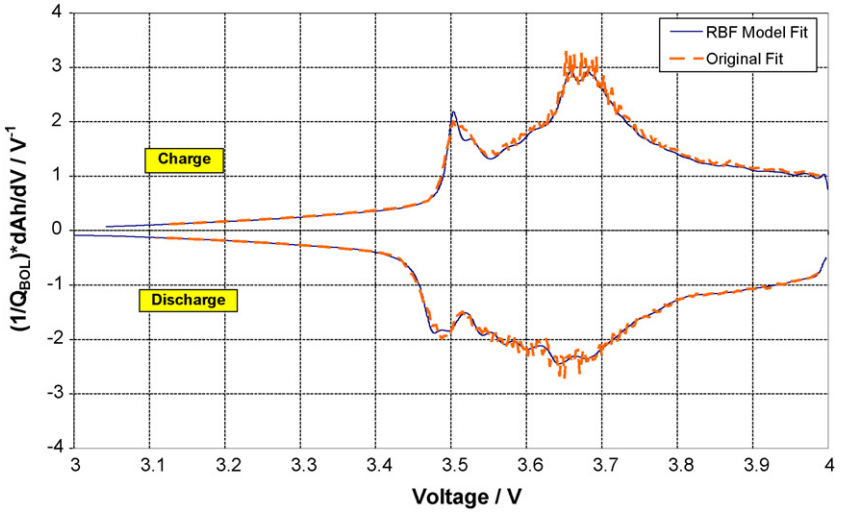

Fig. 9. Comparison of *dQ*/*dV* analysis methods (RBF vs. data reduction) for a Gen3 Variant A 18650 cell at BOL.

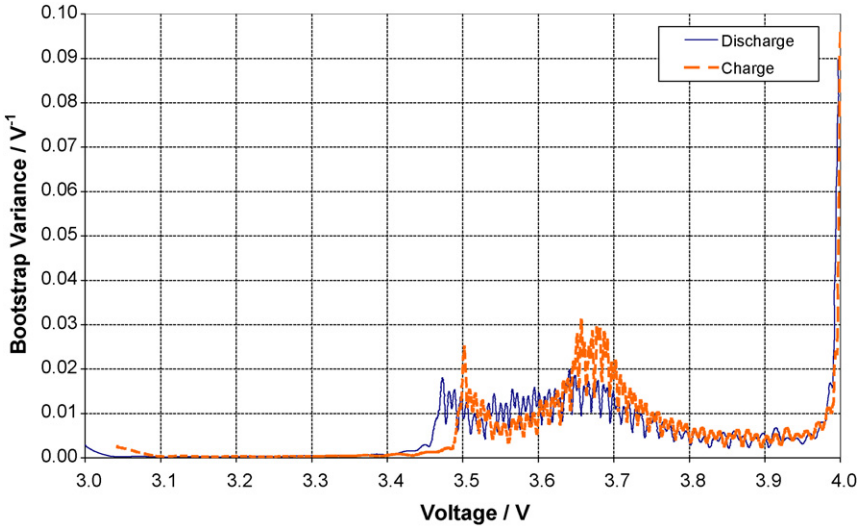

Fig. 10. Bootstrap variance analysis for the *dQ*/*dV* curve of a Gen3 Variant A 18650 cell at BOL.

Table 5
Average bootstrap variance of the representative Gen3 cells.

	Prismatic cell		18650 cell	
	dQ/*dV*	*dV*/*dQ*	*dQ*/*dV*	*dV*/*dQ*
Discharge	3.95 mV^{-1}	0.20 μV	9.36 mV^{-1}	0.35 μV
Charge	6.18 mV^{-1}	0.20 μV	10.85 mV^{-1}	0.39 μV

still yields a very smooth differential signal. Thus, the RBF method can still successfully resolve peaks while making use of the entire voltage dataset despite the increased noise content. As with the Gen2 Baseline cell, the Gen3 18650-size cell shows an initially sharper charge peak followed by a "bump" near 3.5 V (Fig. 9a) or 1.3 mAh cm^{-2}. Similar results were also observed for the representative Gen3 prismatic cell, though the additional "bump" in the initial charge peak was not seen for either the RBF or data reduction method (not shown in this paper).

The corresponding bootstrap error estimation for the same representative 18650-size Gen3 Variant A cell is shown in Fig. 10. As with the Gen2 cells, the variances at the extremes is higher because of how the samples were randomly chosen. A summary of the average bootstrap variances for both the representative Gen3 prismatic and 18650 cells at BOL are summarized in Table 5. The differential capacity curves have an average variance less than ±11 mV^{-1}, and the differential voltage curves have average variances less than ±0.5 μV, indicating a very good model fit for these cells as well. The *dQ*/*dV* variance (Fig. 10) also show increased noise levels at the various peak locations, but the maximum variance is less than 1.5% of the peak amplitude.

4. Summary and conclusions

The use of radial basis functions appears to be a very good, robust methodology for determining battery differential capacity and differential voltage. Unlike the original filtering and data reduction methods, radial basis functions make use of all the available data and allows for an explicit tradeoff between curve detail and noise levels. The model is not overly sensitive to the Gaussian width or number of centers, and once appropriate values have been selected so as to avoid singular matrices and fitting errors (i.e., overfitting or underfitting), respectively, the model can successfully capture the voltage response as a function of time. The derivative of the model can then be used to find a smoothed differential capacity or differential voltage curve. This approach was applied to representative lithium-ion cells of different chemistries and sizes and found to yield smoother results when compared to the original data reduction methods. Another significant advantage of using radial basis functions is the ability to evaluate the uncertainty of the fit using the bootstrap technique. Using 100 randomly sampled datasets, the fitted differential curves generally showed very little variance, thus providing confidence that the model is good. Consequently, radial basis functions should prove useful when identifying and assessing peaks from differential data to isolate contributions from individual electrodes.

Acknowledgements

This work was prepared as an account of work sponsored by an agency of the United States Government under US DOE Contract DE-AC07-05ID14517. Funding for this work was provided by the U.S. DOE Office of Vehicle Technologies (INL) and NSF award #0547616 (MSU). The authors gratefully acknowledge Kevin Gering (INL) and Ira Bloom (ANL) for providing valuable comments.

References

[1] FY2009 Progress Report for Energy Storage Research and Development, U.S. DOE FreedomCAR and Vehicle Technologies Program, January 2009.
[2] Advanced Technology Development Program for Lithium-Ion Batteries: Gen 2 Performance Evaluation Final Report, INL/EXT-05-00913, July 2006.
[3] FreedomCAR Battery Test Manual for Power-Assist Hybrid Electric Vehicles, DOE/ID-11069, October 2003.
[4] PNGV Battery Test Manual, DOE/ID-10597, Revision 3, February 2001.
[5] I. Bloom, A.N. Jansen, D.P. Abraham, J. Knuth, S.A. Jones, V.S. Battaglia, G.L. Henriksen, Differential voltage analyses of high-power, lithium-ion cells. 1. Technique and application, J. Power Sources 139 (2005) 295–303.
[6] I. Bloom, J. Christophersen, K. Gering, Differential voltage analyses of high-power lithium-ion cells. 2. Applications, J. Power Sources 139 (2005) 304–313.
[7] I. Bloom, J.P. Christophersen, D.P. Abraham, K.L. Gering, Differential voltage analyses of high-power lithium-ion cells. 3. Another anode phenomenon, J. Power Sources 157 (2006) 537–542.
[8] I. Bloom, L.K. Walker, J.K. Basco, D.P. Abraham, J.P. Christophersen, C.D. Ho, Differential voltage analyses of high-power lithium-ion cells. 4. Cells containing NMC, J. Power Sources 195 (2010) 877–882.
[9] D.P. Abraham, J.L. Knuth, D.W. Dees, I. Bloom, J.P. Christophersen, Performance degradation of high-power lithium-ion cells—electrochemistry of harvested electrodes, J. Power Sources 170 (2007) 465–475.

[10] D.P. Abraham, S.D. Poppen, A.N. Jansen, J. Liu, D.W. Dees, Application if a lithium-tin reference electrode to determine electrode contributions to impedance rise in high-power lithium-ion cells, Electrochim. Acta 49 (2004) 4763–4775.
[11] N. Gershenfeld, The Nature of Mathematical Modeling, Cambridge University Press, Cambridge, UK, 1999.
[12] L. Ljung, System Identification: Theory for the User, second ed., Prentice-Hall, Upper Saddle River, NJ, 1999.
[13] R. Johansson, System Modeling and Identification, Prentice-Hall, Englewood Cliffs, NJ, 1993.
[14] A.M. Zoubir, D.R. Iskander, Bootstrapping Techniques for Signal Processing, Cambridge University Press, Cambridge, UK, 2004.